Synthesis of Phosphido-bridged Ruthenium–Manganese Complexes; X-Ray Crystal Structures of $[RuMn(\mu\text{-}H)(\mu\text{-}PPh_2)(\eta^5\text{-}C_5H_5)(CO)_5]$, $[Ru_2(\mu\text{-}H)(\mu\text{-}PPh_2)(\eta^5\text{-}C_5H_5)_2(CO)_2]$ and $[RuMn_2(\mu\text{-}H)(\mu\text{-}PPh_2)_2(\eta^5\text{-}C_5H_5)(CO)_9]$ †

Andrew J. M. Caffyn, Martin J. Mays* and Paul R. Raithby
University Chemical Laboratory, Lensfield Road, Cambridge CB2 1EW, UK

The complex $[RuMn(\eta^5\text{-}C_5H_5)(CO)_7]$ **1** has been synthesised in 70% yield from the reaction of $[Ru(\eta^5\text{-}C_5H_5)(CO)_2I]$ with $Na[Mn(CO)_5]$. Photolytic reaction of **1** with PPh_2H gives the new complexes $[RuMn(\mu\text{-}H)(\mu\text{-}PPh_2)(\eta^5\text{-}C_5H_5)(CO)_5]$ **2**, $[Mn_2(\mu\text{-}H)(\mu\text{-}PPh_2)(CO)_7(PPh_2H)]$ **3**, *trans*- and *cis*-$[Ru_2(\mu\text{-}H)(\mu\text{-}PPh_2)(\eta^5\text{-}C_5H_5)_2(CO)_2]$ **4a** and **b**, $[RuMn_2(\mu\text{-}H)(\mu\text{-}PPh_2)_2(\eta^5\text{-}C_5H_5)(CO)_9]$ **5** and $[RuMn_2(\mu\text{-}H)(\mu\text{-}PPh_2)_2(\eta^5\text{-}C_5H_5)(CO)_8(PPh_2H)]$ **6** together with the known complexes $[Mn_2(\mu\text{-}H)(\mu\text{-}PPh_2)(CO)_8]$ and $[Ru_2(\eta^5\text{-}C_5H_5)_2(CO)_4]$. The crystal structures of **2**, **4a** and **5** have been determined. Structures are proposed for the other new complexes and the mechanism of the photolytic reaction of **1** with PPh_2H is discussed.

The oxidative addition of secondary phosphines, PR_2H (R = alkyl or aryl), to dinuclear carbonyl complexes has proved an effective way of synthesising homodinuclear transition-metal complexes containing both bridging phosphido- and hydrido-ligands.[1–8] The same method has been used to prepare a heterodinuclear complex of this type, $[MoMn(\mu\text{-}H)(\mu\text{-}PPh_2)(\eta^5\text{-}C_5H_5)(CO)_6]$, from the photolytic reaction of $[MoMn(\eta^5\text{-}C_5H_5)(CO)_8]$ with PPh_2H.[9]

We have previously studied the reactions of the above molybdenum–manganese complex with unsaturated organic molecules,[10–12] and, in an attempt to extend these studies, we investigated the possibility of synthesising the corresponding ruthenium–manganese complex, $[RuMn(\mu\text{-}H)(\mu\text{-}PPh_2)(\eta^5\text{-}C_5H_5)(CO)_5]$ **2** from the reaction of $[RuMn(\eta^5\text{-}C_5H_5)(CO)_7]$ **1** with PPh_2H. The results presented in this paper show, however, that the photolytic reaction of **1** with PPh_2H is less specific than that leading to the corresponding molybdenum–manganese complex (which is obtained in *ca.* 40% yield) and **2** is only a minor product. Complex **2**, which is the first phosphido-hydrido-bridged ruthenium–manganese species to be reported, has, however, been fully characterised together with two new trinuclear phosphido-bridged ruthenium–manganese complexes and a number of homonuclear manganese and ruthenium complexes which are also obtained as reaction products.

Results and Discussion

(*a*) *Synthesis and Characterisation of the New Complexes.*—Complex **1** was synthesised by a method similar to that used for $[FeMn(\eta^5\text{-}C_5H_5)(CO)_7]$.[13] This involved the attack of a nucleophilic metal anion on a metal carbonyl halide complex, resulting in the formation of a bimetallic complex and displacement of an inorganic salt. By this means yellow **1** was produced in 70% yield from reaction of $[Ru(\eta^5\text{-}C_5H_5)(CO)_2I]$ with $Na[Mn(CO)_5]$ in tetrahydrofuran (thf) at 328 K.

Complex **1** is assigned the structure shown on the basis of IR, ^1H and ^{13}C NMR and mass spectrometry and microanalysis (see Experimental section). The IR (ν_{CO}) spectrum is very similar to those of $[FeMn(\eta^5\text{-}C_5H_5)(CO)_7]$[13] and $[RuMn(\eta^5\text{-}C_8H_7)(CO)_7]$,[14] showing only terminal ν_{CO} absorption bands. In the ^{13}C NMR spectrum at 243 K the only CO resonance observed was a broadened singlet centred at δ 216. It can thus be concluded that CO site exchange in **1** is rapid on the NMR time-scale, at least at 243 K. A broadened singlet centred at δ 220 was

† Pentacarbonyl-1κ^4C,2κC-2(η^5)-cyclopentadienyl-μ-diphenylphosphido-μ-hydrido-manganeseruthenium (*Mn–Ru*), *trans*-μ-diphenylphosphido-μ-hydrido-bis[carbonyl(η^5-cyclopentadienyl)ruthenium] (*Ru–Ru*), and nonacarbonyl-1κ^4C,2κ^3C,3κ^3C-3(η^5)-cyclopentadienyl-bis(μ-diphenylphosphido)-1:2κ^2P; 2:3κ^2P-μ-hydrido-1:2κ^2H-dimanganeseruthenium (*Mn–Mn*).

Supplementary data available: see Instructions for Authors, *J. Chem. Soc., Dalton Trans.*, 1991, Issue 1, pp. xviii–xxii.

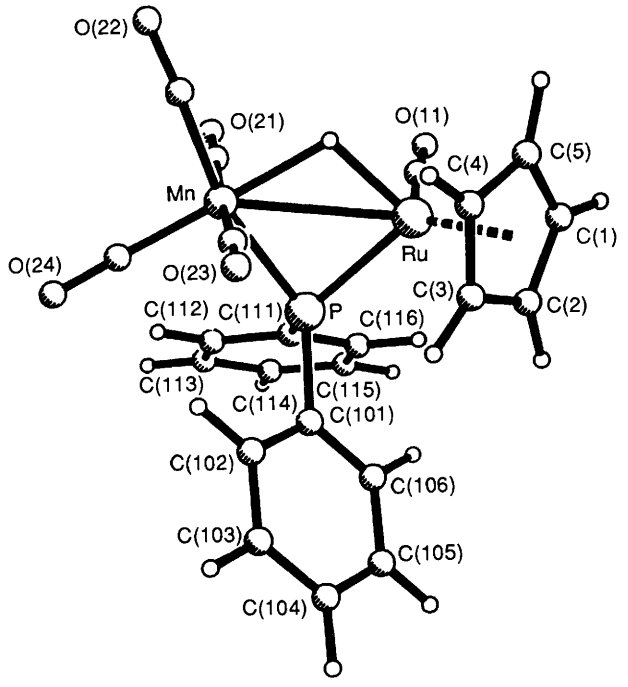

Fig. 1 Molecular structure of $[RuMn(\mu\text{-}H)(\mu\text{-}PPh_2)(\eta^5\text{-}C_5H_5)(CO)_5]$ **2** showing the crystallographic numbering

also observed throughout the temperature range 298–200 K in the ^{13}C NMR spectrum of a ^{13}CO-enriched sample of $[FeMn(\eta^5\text{-}C_5H_5)(CO)_7]$.[15]

When complex **1** and PPh_2H were heated together in toluene at 353 K and then refluxed for 18 h **1** decomposed slowly; IR monitoring did not reveal the presence of new ruthenium–manganese products at any stage. In contrast, UV irradiation of a toluene solution of **1** in the presence of 2 equivalents of PPh_2H produced a range of products, all isolated in low to moderate yields (see Experimental section) which, in order of elution, were as follows: $[Mn_2(\mu\text{-}H)(\mu\text{-}PPh_2)(CO)_8]$,[5,16] $[RuMn(\mu\text{-}H)(\mu\text{-}PPh_2)(\eta^5\text{-}C_5H_5)(CO)_5]$ **2**, $[Mn_2(\mu\text{-}H)(\mu\text{-}PPh_2)(CO)_7(PPh_2H)]$ **3**, *trans*-$[Ru_2(\mu\text{-}H)(\mu\text{-}PPh_2)(\eta^5\text{-}C_5H_5)_2(CO)_2]$ **4a**, *cis*-$[Ru_2(\mu\text{-}H)(\mu\text{-}PPh_2)(\eta^5\text{-}C_5H_5)_2(CO)_2]$ **4b**, $[RuMn_2(\mu\text{-}H)(\mu\text{-}PPh_2)_2(\eta^5\text{-}C_5H_5)(CO)_9]$ **5**, $[RuMn_2(\mu\text{-}H)(\mu\text{-}PPh_2)_2(\eta^5\text{-}C_5H_5)(CO)_8(PPh_2H)]$ **6** and $[Ru_2(\eta^5\text{-}C_5H_5)_2(CO)_4]$.[17] All the above complexes have been characterised spectroscopically and, in addition, the solid-state structures of **2**, **4a** and **5** have been determined by X-ray diffraction.

Crystal structure of complex **2**. crystals of complex **2** suitable for an X-ray diffraction study were grown from dichloromethane–hexane (1:1) solution. The molecular structure is shown in Fig. 1. Table 1 lists selected bond lengths and angles. The structure is pseudoisomorphous with the related iron–manganese complex $[FeMn(\mu\text{-}H)(\mu\text{-}PPh_2)(\eta^5\text{-}C_5H_5)(CO)_5]$.[18] The two metal atoms are bridged by a PPh_2 group and by a hydride ligand which was located and refined. The Mn atom is further bonded to four carbonyl ligands such that, if the metal–metal bond is ignored, it is essentially octahedrally co-ordinated. The Ru atom is additionally co-ordinated by a cyclopentadienyl and a carbonyl ligand with an irregular geometry around the metal centre.

The Ru–Mn bond is, as expected, rather longer at 2.894(1) Å than the Fe–Mn bond in $[FeMn(\mu\text{-}H)(\mu\text{-}PPh_2)(\eta^5\text{-}C_5H_5)(CO)_5]$ [2.806(1) Å][18] but is slightly shorter than the metal–metal bond length in either of the corresponding homodinuclear complexes $[Mn_2(\mu\text{-}H)(\mu\text{-}PPh_2)(CO)_8]$[5,19] or $[Ru_2(\mu\text{-}H)(\mu\text{-}PPh_2)(\eta^5\text{-}C_5H_5)_2(CO)_2]$ (see below). No other Ru–Mn distances in dinuclear complexes are available in comparison but Ru–Mn distances of 2.828(2) and 2.848(2) Å were found in the trinuclear complex $[Ru_2Mn(\mu_3\text{-}PC_6H_{11})(\eta^5\text{-}C_5H_5)(CO)_8]$.[20]

Table 1 Selected bond lengths (Å) and angles (°) for $[RuMn(\mu\text{-}H)(\mu\text{-}PPh_2)(\eta^5\text{-}C_5H_5)(CO)_5]$ **2**

Mn–Ru	2.894(1)	H(12)–Ru	1.74(6)
P–Ru	2.277(1)	C(1)–Ru	2.208(7)
C(2)–Ru	2.208(8)	C(3)–Ru	2.235(9)
C(4)–Ru	2.251(7)	C(5)–Ru	2.258(7)
C(11)–Ru	1.840(7)	H(12)–Mn	1.86(6)
P(1)–Mn	2.278(2)	C(21)–Mn	1.851(7)
C(22)–Mn	1.821(6)	C(23)–Mn	1.854(7)
C(24)–Mn	1.783(6)	C(101)–P	1.836(4)
C(111)–P	1.840(5)	C(2)–C(1)	1.387(12)
C(5)–C(1)	1.397(10)	C(3)–C(2)	1.405(11)
C(4)–C(3)	1.372(12)	C(5)–C(4)	1.406(13)
P(1)–Ru–Mn	50.6(1)	P–Ru–H(12)	88(2)
H(12)–Ru–Mn	38(2)	H(12)–Mn–Ru	35(2)
P–Mn–H(12)	85(2)	P–Mn–Ru	50.6(1)
Mn–H(12)–Ru	107(3)	Mn–P–Ru	78.9(1)
C(5)–C(1)–C(2)	109.0(7)	C(3)–C(2)–C(1)	107.6(6)
C(4)–C(3)–C(2)	107.8(8)	C(5)–C(4)–C(3)	109.4(7)
C(4)–C(5)–C(1)	106.2(7)		

In contrast to the analogous FeMn complex,[18] the phosphido ligand in **2** bridges the metal–metal bond symmetrically, with Ru–P and Mn–P bond lengths of 2.277(1) and 2.278(2) Å respectively. The hydride ligand was observed to lie in the Ru–Mn–P plane. The carbonyl ligand bonded to ruthenium is almost perpendicular to this plane, as are the two axial carbonyls on manganese [CO(21) and CO(23)]. As observed for other dinuclear phosphido, hydrido-bridged complexes containing $Mn(CO)_4$ units,[12,18,19,21] the Mn–CO bond lengths vary according to the π acidity of the *trans* ligand. The shortest Mn–CO distance, 1.783(6) Å, is observed for CO(24) *trans* to the bridging hydride ligand (the weakest π acid co-ordinated to manganese). The next shortest Mn–CO distance is 1.821(6) Å for CO(22), *trans* to the phosphido group. The two axial carbonyls are bound least strongly as they lie *trans* to each other (the carbonyls being the strongest π acids).

The IR (ν_{CO}) spectrum of complex **2** in hexane shows four terminal carbonyl absorption bands and is very similar to that observed for $[FeMn(\mu\text{-}H)(\mu\text{-}PPh_2)(\eta^5\text{-}C_5H_5)(CO)_5]$.[18] At 215 K separate ^{13}C NMR resonances are observed for each of the five carbonyl groups. At 298 K, however, only the resonance due to the ruthenium-bonded carbonyl ligand remains visible. This could be due either to increased broadening of the four manganese-bonded carbonyl signals, resulting from the slowing down of quadrupolar relaxation of ^{55}Mn nuclei at higher temperatures,[22a] or possibly to localised scrambling of the carbonyl ligands on manganese.

Complex **3** was characterised by IR, ^1H and ^{31}P NMR and mass spectrometry and microanalysis. These data suggest that it can be formulated as $[Mn_2(\mu\text{-}H)(\mu\text{-}PPh_2)(CO)_7(PPh_2H)]$, analogous to the previously reported phosphine substitution products $[Mn_2(\mu\text{-}H)(\mu\text{-}PPh_2)(CO)_7(PR_3)]$ (R = Ph or OMe).[5]

Crystal structure of complex **4a**. Crystals of complex **4a** suitable for an X-ray diffraction study were grown from dichloromethane–hexane (1:1) solution. The molecular structure is shown in Fig. 2 and Table 2 lists selected bond lengths and angles. The molecule has C_2 symmetry with the two-fold crystallographic symmetry axis passing through the phosphorus atom, the centre of the Ru–Ru bond and the hydride ligand. The two ruthenium atoms are symmetrically bridged by a PPh_2 and a hydride ligand which was located and refined. Each metal atom is additionally ligated by one cyclopentadienyl and one carbonyl ligand, each being disposed *trans* to the corresponding ligand on the other metal atom.

The Ru–Ru bond length of 2.908(1) Å is consistent with a hydrogen-bridged single bond,[22b] although it is considerably longer than the 2.735(2) Å observed for $[Ru_2(\eta^5\text{-}C_5H_5)_2(CO)_4]$.[23] The Ru–P bond lengths of 2.292(1) Å compare with

a Ru–P bond length of 2.277(1) Å for complex **2** and the Ru–P–Ru bite angle is 78.7(1)° almost the same as the corresponding angle in **2** [78.9(1)°]. The carbonyl ligands lie *cis* to the Ru–Ru bond with C(1)–Ru–Ru *ca.* 93°. The Ru–C(1) bond distances of 1.856(5) Å compare with Ru–C bond distances of 1.855(14) Å for the terminal carbonyl ligands in $[Ru_2(\eta^5\text{-}C_5H_5)_2(CO)_4]$.[23]

Infrared spectroscopy proved to be the easiest way to differentiate between the two isomers of complex **4**. Both complexes **4a** and **4b** are insoluble in hexane but in dichloromethane solution one strong carbonyl absorption bond is observed for **4a** (1919 cm^{-1}) and **4b** (1956 cm^{-1}). The latter band, in particular, was broad. One strong and one weak IR-active terminal carbonyl band are predicted for a *cis*-$[Ru_2(\eta^5\text{-}C_5H_5)_2(CO)_2]$ unit, arising from the symmetric and antisymmetric stretching of the pair of carbonyls.[24] In this instance it is possible that the predicted weak band is obscured. There appeared to be no tendency for the complexes **4** to interconvert, in that no traces of **4b** were detected by IR spectroscopy when a dichloromethane solution of **4a** was allowed to stand at 293 K for 1 week.

A diiron analogue of complex **4** has been reported[25] but no X-ray structure determination was undertaken.

Crystal structure of complex **5**. Crystals of complex **5** suitable for an X-ray diffraction study were grown from dichloromethane–hexane (1:1) solution. The molecular structure is shown in Fig. 3 and Table 3 lists selected bond lengths and angles.

The molecular structure is formally related to that of $[Mn_2(\mu\text{-}H)(\mu\text{-}PPh_2)(CO)_8]$[19,20] with the metallophosphine $[Ru(\eta^5\text{-}C_5H_5)(CO)_2(PPh_2)]$ having replaced a carbonyl ligand *trans* to the μ-PPh_2 group at one of the manganese centres. Thus the Mn(1)–Mn(2) bond length of 2.961(2) Å is close to that observed for $[Mn_2(\mu\text{-}H)(\mu\text{-}PPh_2)(CO)_8]$ and lies within the range expected for Mn–Mn single bonds.[26] The Mn(2)–P(2) distance of 2.297(2) Å is *ca.* 0.06 Å longer than the Mn(1)–P(2) distance which is consistent with more π-back donation of electron density to P(2) from Mn(1) than from Mn(2). This can be rationalised on the basis of Mn(1) being co-ordinated by only three carbonyl ligands whereas Mn(2) is co-ordinated by four. The $Ru(\eta^5\text{-}C_5H_5)(CO)_2(PPh_2)$ ligand on Mn(1) is likely to be a better σ donor and poorer π acceptor than the fourth carbonyl ligand which it formally replaces, giving rise to a higher electron density on Mn(1) than on Mn(2). The Mn(1)–P(2)–Mn(2) bite angle is 81.5(1)°, close to that of 80.3(1) Å for $[Mn_2(\mu\text{-}H)(\mu\text{-}PPh_2)(CO)_8]$. The bridging hydride in **5** is in the Mn(1)–Mn(2)–P(2) plane, displaced such that it lies closer to Mn(2) by *ca.* 0.07 Å than to Mn(1). The Mn–CO bond lengths for both manganese atoms show the expected variation with π acidity of the *trans* ligand. Thus the shortest bond lengths are observed for the carbonyls *trans* to the bridging hydride ligand (the weakest π acid). The two axial carbonyls on each manganese are the least strongly bound.

There is clearly no direct interaction between the metal atoms Mn(1) and Ru. Thus the interatomic separation is 4.058(2) Å and the phosphido group bridging these two metal atoms has a

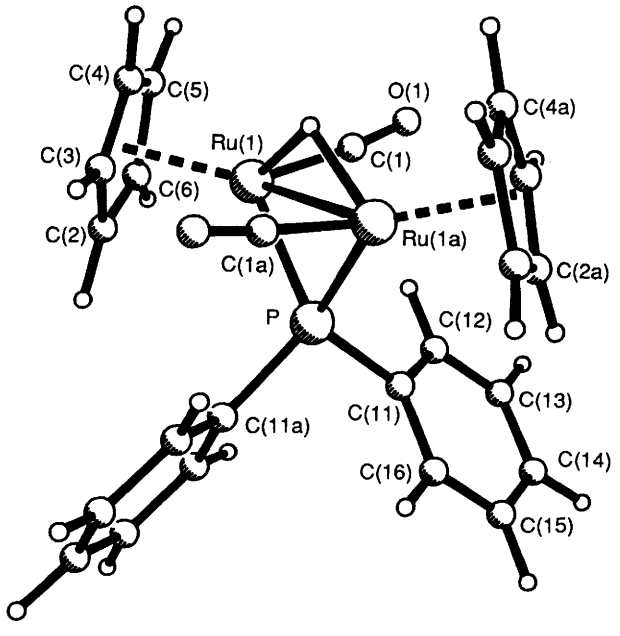

Fig. 2 Molecular structure of *trans*-$[Ru_2(\mu\text{-}H)(\mu\text{-}PPh_2)(\eta^5\text{-}C_5H_5)_2(CO)_2]$ **4a** showing the crystallographic numbering

Table 2 Selected bond lengths (Å) and angles (°) for $[Ru_2(\mu\text{-}H)(\mu\text{-}PPh_2)(\eta^5\text{-}C_5H_5)_2(CO)_2]$ **4a**

P–Ru(1)	2.292(1)	H(1)–Ru(1)	2.79(4)
C(1)–Ru(1)	1.856(5)	C(2)–Ru(1)	2.256(4)
C(3)–Ru(1)	2.264(5)	C(4)–Ru(1)	2.259(5)
C(5)–Ru(1)	2.237(4)	C(6)–Ru(1)	2.219(5)
Ru(1)–Ru(1a)	2.908(1)	C(3)–C(2)	1.352(8)
C(6)–C(2)	1.461(9)	C(4)–C(3)	1.340(9)
C(5)–C(4)	1.374(8)	C(6)–C(5)	1.445(9)
P–Ru(1)–H(1)	86(2)	C(1)–Ru(1)–H(1)	88.5(2)
C(1)–Ru(1)–P	96.7(1)	Ru(1)–H(1)–Ru(1a)	109(3)
Ru(1)–P–Ru(1a)	78.7(1)	C(11)–P–Ru(1)	124.4(1)
C(11)–P–C(11a)	100.5(2)	C(6)–C(2)–C(3)	107.2(5)
C(4)–C(3)–C(2)	111.3(6)	C(5)–C(4)–C(3)	109.7(6)
C(6)–C(5)–C(4)	107.6(5)	C(5)–C(6)–C(2)	104.2(5)

Table 3 Selected bond lengths (Å) and angles (°) for $[RuMn_2(\mu\text{-}H)(\mu\text{-}PPh_2)_2(\eta^5\text{-}C_5H_5)(CO)_9]$ **5**

P(1)–Ru	2.398(2)	C(1)–Ru	2.249(11)
C(2)–Ru	2.228(9)	C(3)–Ru	2.254(8)
C(4)–Ru	2.252(10)	C(5)–Ru	2.237(11)
C(11)–Ru	1.868(9)	C(12)–Ru	1.872(9)
Mn(2)–Mn(1)	2.961(2)	H(23)–Mn(1)	1.76(6)
P(1)–Mn(1)	2.358(2)	P(2)–Mn(1)	2.237(2)
C(21)–Mn(1)	1.831(8)	C(22)–Mn(1)	1.790(9)
C(23)–Mn(1)	1.824(8)	H(23)–Mn(2)	1.69(5)
P(2)–Mn(2)	2.297(2)	C(31)–Mn(2)	1.844(9)
C(32)–Mn(2)	1.851(9)	C(33)–Mn(2)	1.777(9)
C(34)–Mn(2)	1.854(9)	C(101)–P(1)	1.856(5)
C(111)–P(1)	1.856(4)	C(201)–P(2)	1.838(5)
C(211)–P(2)	1.842(5)	C(2)–C(1)	1.413(15)
C(5)–C(1)	1.383(16)	C(3)–C(2)	1.388(13)
C(4)–C(3)	1.387(14)	C(5)–C(4)	1.414(16)
C(11)–Ru–P(1)	92.9(3)	C(12)–Ru–P(1)	90.9(3)
C(12)–Ru–C(11)	93.2(4)	H(23)–Mn(1)–Mn(2)	30(2)
P(1)–Mn(1)–Mn(2)	107.8(1)	H(23)–Mn(1)–P(1)	78(2)
P(2)–Mn(1)–Mn(2)	50.1(1)	H(23)–Mn(1)–P(2)	80(2)
P(2)–Mn(1)–P(1)	157.9(1)	C(21)–Mn(1)–Mn(2)	92.0(2)
C(21)–Mn(1)–P(1)	89.4(2)	C(21)–Mn(1)–P(2)	90.0(2)
C(22)–Mn(1)–Mn(2)	151.5(2)	C(22)–Mn(1)–P(1)	100.6(2)
C(22)–Mn(1)–P(2)	101.4(2)	C(22)–Mn(1)–C(21)	86.3(3)
C(23)–Mn(1)–Mn(2)	95.0(2)	C(23)–Mn(1)–P(1)	93.1(2)
C(23)–Mn(1)–P(2)	90.7(2)	C(23)–Mn(1)–C(21)	171.5(4)
C(23)–Mn(1)–C(22)	85.3(3)	H(23)–Mn(2)–Mn(1)	32(2)
P(2)–Mn(2)–Mn(1)	48.4(1)	H(23)–Mn(2)–P(2)	80(2)
C(31)–Mn(2)–Mn(1)	115.4(3)	C(32)–Mn(2)–P(2)	163.6(3)
C(32)–Mn(2)–Mn(1)	91.0(3)	C(32)–Mn(2)–P(2)	92.5(3)
C(32)–Mn(2)–C(31)	89.4(4)	C(33)–Mn(2)–Mn(1)	147.8(3)
C(33)–Mn(2)–P(2)	99.5(3)	C(33)–Mn(2)–C(31)	96.8(4)
C(33)–Mn(2)–C(32)	89.7(4)	C(34)–Mn(2)–Mn(1)	88.6(3)
C(34)–Mn(2)–P(2)	88.8(3)	C(34)–Mn(2)–C(31)	88.9(4)
C(34)–Mn(2)–C(32)	177.8(4)	C(34)–Mn(2)–C(33)	91.8(4)
Mn(2)–H(23)–Mn(1)	118(3)	Mn(1)–P(1)–Ru	117.1(1)
Mn(2)–P(2)–Mn(1)	81.5(1)	C(5)–C(1)–C(2)	107.6(9)
C(3)–C(2)–C(1)	107.9(9)	C(4)–C(3)–C(2)	108.7(8)
C(5)–C(4)–C(3)	107.4(9)	C(4)–C(5)–C(1)	108.3(9)

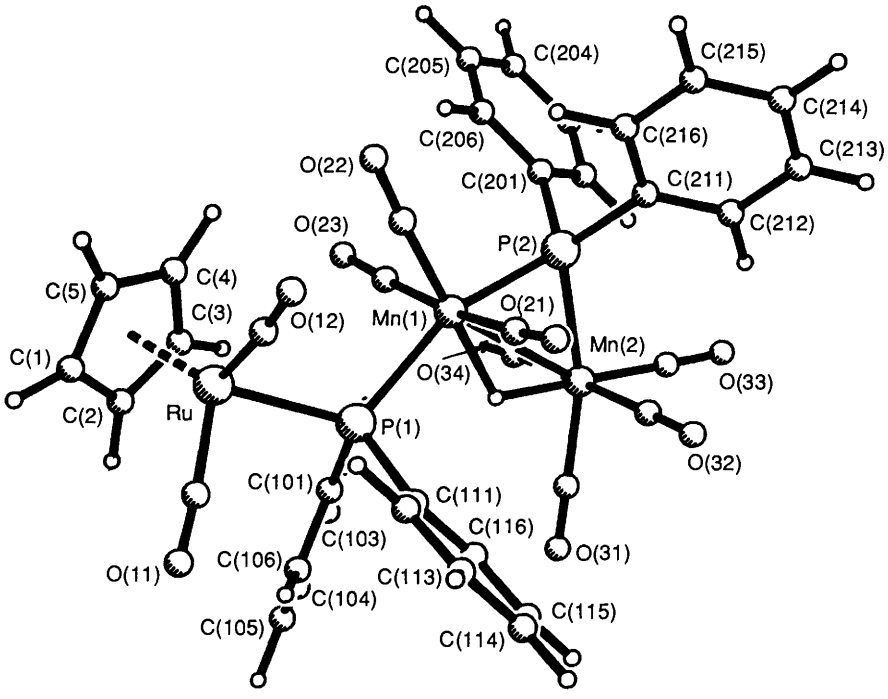

Fig. 3 Molecular structure of $[RuMn_2(\mu\text{-}H)(\mu\text{-}PPh_2)_2(\eta^5\text{-}C_5H_5)(CO)_9]$ **5** showing the crystallographic numbering

Mn–P–Ru bite angle of 117.1(1)° which is typical for such a situation.[27] The Ru–P(1) and Mn(1)–P(1) distances of 2.398(2) and 2.358(2) Å respectively are significantly longer than the corresponding Ru–P and Mn–P distances [2.277(1) and 2.278(2) Å] in complex **2**.

The IR (ν_{CO}) spectrum of complex **5** in hexane solution shows seven terminal carbonyl absorption bands. In the ^1H NMR spectrum the hydride resonance shows coupling to both phosphorus atoms, appearing as a doublet of doublets at δ −15.68. The $^{31}P\text{-}\{^1H\}$ NMR spectrum is consistent with the solid-state structure. The phosphorus resonance due to the phosphido group bridging the Mn–Mn bond appears at δ 26.4, whereas the resonance due to the phosphido group linking Mn(1) to Ru appears at δ −97.4. This higher-field resonance is consistent with that expected for a phosphido ligand bridging two metals not joined by a metal–metal bond. Numerous correlations have shown that $\mu\text{-}PR_2$ ligands bridging metal–metal bonds generally have lower-field ^{31}P NMR chemical shifts (δ 50 to 200) relative to the shifts observed for $\mu\text{-}PR_2$ ligands where no direct metal–metal interactions are present (δ −50 to −300).[28–31]

Complex **6** gives a fast-atom bombardment (FAB) mass spectrum which shows a molecular ion peak at *m/z* 1058 with peaks corresponding to the loss of *n*CO (*n* = 3–8). This is consistent with a formulation of $[RuMn_2(\mu\text{-}H)(\mu\text{-}PPh_2)_2(\eta^5\text{-}C_5H_5)(CO)_8(PPh_2H)]$. The IR ($\nu_{CO}$) spectrum of the complex in hexane is similar to that of **5**, but shows one less carbonyl absorption band.

The $^{31}P\text{-}\{^1H\}$ NMR spectrum of complex **6** is consistent with the presence of the same metal framework as observed for **5**. A low-field phosphorus resonance at δ 25.6 is assigned to a PPh_2 group bridging a Mn–Mn bond. Two singlet high-field resonances were observed at δ −102.1 and −106.4. When the proton decoupler was switched off the resonance at δ −102.1 split into a doublet, indicating that it can be assigned to a PPh_2H group. The signal at δ −106.4 can therefore be ascribed to a $\mu\text{-}PPh_2$ group linking ruthenium and manganese atoms which are not otherwise bonded together.

If complex **6** is formulated as a diphenylphosphine-substituted derivative of **5**, then the PPh_2H ligand could be substituted on any of the three metal atoms (Fig. 4). In the ^1H NMR spectrum of **6** the PPh_2H proton resonance appears as a doublets of doublets centred at δ 6.46 with $^1J(PH)$ 377 Hz and $^3J(PH)$ 11.9 Hz. This observation militates against structure **B** and in favour of **A** or **C**. For structure **B** two, three-bond P–H couplings as well as a large one-bond P–H coupling would be expected. For **A** and **C** only one three-bond P–H coupling together with a larger one-bond P–H coupling would be predicted and this is what is observed. The hyride ligand gives rise to a doublet of doublets centred at δ −15.48 with $^2J(PH)$ 32 Hz and $^2J(P'H)$ 21 Hz. For **B** and **C** three $^2J(PH)$ couplings would have been expected, two to the $\mu\text{-}PPh_2$ groups and another to a manganese-bonded PPh_2H ligand. On the other hand for **A** the PPh_2H ligand is too remote to be likely to show coupling to the μ-H ligand and this is again consistent with the observed spectrum. On this basis complex **6** is assigned structure **A** with the PPh_2H ligand bonded to the ruthenium atom.

(*b*) *Mechanism of the Photolytic Reaction of Complex* **1** *with* PPh_2H.—The diversity of products obtained in this reaction, together with the observation that the ratio and concentration of the reactants and the reaction time all affect the product distribution, indicate a complex reaction mechanism. Nevertheless some indication of the primary photoprocesses involved can be obtained from a consideration of the range of products formed.

As in the photolytic reaction of $[MoMn(\eta^5\text{-}C_5H_5)(CO)_8]$ and PPh_2H,[11] two alternative initial steps can be envisaged (Scheme 1). These are (*i*) direct photochemical substitution of CO by PPh_2H and (*ii*) homolytic metal–metal bond cleavage followed by substitution of CO by PPh_2H in one or both of the radicals. The fact that considerable quantities of homolysis products were isolated from the reaction indicates that the latter process is significant.

Work on the analogous $[FeMn(\eta^5\text{-}C_5H_5)(CO)_7]$ system has shown that photochemical metal–metal bond homolysis and CO loss are competitive processes at room temperature.[15] It was found that CO loss occurred exclusively on manganese; reaction with phosphines then generated the complexes $[(OC)_2$-

$(\eta^5\text{-}C_5H_5)FeMn(CO)_4(PR_3)]$ (R = Ph or OPh). Furthermore, these complexes were found to be labile with respect to Fe–Mn bond cleavage. If the Ru–Mn system behaves in a similar way, photogenerated $[(OC)_2(\eta^5\text{-}C_5H_5)RuMn(CO)_4(PPh_2H)]$ **X** (Scheme 1) could produce $[Ru(\eta^5\text{-}C_5H_5)(CO)_2]^\bullet$ and $[Mn(CO)_4(PPh_2H)]^\bullet$. Alternatively, further photochemical CO loss from **X** would allow intramolecular oxidative addition of a P–H bond of the co-ordinated PPh_2H ligand to yield complex **2**. The formation of $[Mn_2(\mu\text{-}H)(\mu\text{-}PPh_2)(CO)_8]$ and $[Mn_2(\mu\text{-}H)(\mu\text{-}PPh_2)(CO)_7(PPh_2H)]$ probably occurs *via* combination of $[Mn(CO)_5]^\bullet$ and $[Mn(CO)_4(PPh_2H)]^\bullet$, or of two $[Mn(CO)_4(PPh_2H)]^\bullet$ radicals respectively, followed by CO loss and oxidative addition of co-ordinated PPh_2H. The relative high yield of these dimanganese products suggests that $[Mn(CO)_4(PPh_2H)]^\bullet$ is readily formed under the reaction conditions whereas the low yields of **4a** and **4b** suggest that $[Ru(\eta^5\text{-}C_5H_5)(CO)(PPh_2H)]^\bullet$ is formed to a lesser extent. Studies on the photochemical substitution of CO by PR_3 (R = Ph or OMe) in $[Fe_2(\eta^5\text{-}C_5H_5)_2(CO)_4]$ have shown that the most likely pathway is generation of $[Fe(\eta^5\text{-}C_5H_5)(CO)_2]^\bullet$, substitution of PR_3 for CO at the radical stage and radical recombination.[32] Formation of **4a** and **4b** by the route shown in Scheme 1 is therefore reasonable.

There are many possible routes to complexes **5** and **6** and it is not possible to draw any conclusions from this work as to which is preferred.

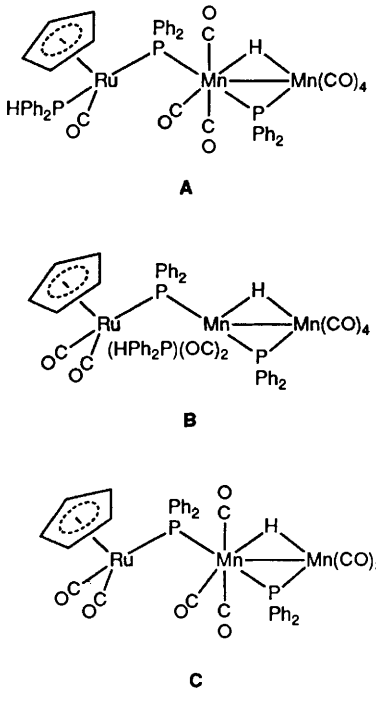

Fig. 4 Possible structures for $[RuMn_2(\mu\text{-}H)(\mu\text{-}PPh_2)_2(\eta^5\text{-}C_5H_5)(CO)_8(PPh_2H)]$ **6**

Experimental

All reactions were carried out under a nitrogen atmosphere in N_2-saturated solvents distilled from the appropriate drying agent and stored over 4 Å molecular sieves. Infrared spectra were recorded in solution in 0.5 mm NaCl cells using a Perkin-Elmer 983 instrument, electron-impact and negative-ion fast-atom bombardment mass spectra on a Kratos MS902 or MS890 instrument using tris(perfluoroheptyl)-1,3,5-triazine as calibrant. Hydrogen-1, ^{13}C and ^{31}P NMR spectra were recorded in CD_2Cl_2, $CDCl_3$ or CD_3COCD_3 solution on Bruker WM250 or AM400 spectrometers. The solvent resonance was used as internal standard, except for ^{31}P where chemical shifts are given relative to $P(OMe)_3$ with upfield shifts negative. Elemental analyses were performed at Cambridge. Preparative thin-layer chromatography (TLC) was carried out on commercial Merck plates coated with a 0.25 mm layer of silica. The complexes $Na[Mn(CO)_5]$[33] and $[Ru(\eta^5\text{-}C_5H_5)(CO)_2I]$[34] were prepared by the literature methods. Photolysis experiments were conducted in a glass vessel with a quartz inner tube containing a Hanovia medium-pressure UV lamp (125 W).

Synthesis of $[RuMn(\eta^5\text{-}C_5H_5)(CO)_7]$ **1**.—A solution of $Na[Mn(CO)_5]$ (0.69 g, 2.2 mmol) and $[Ru(\eta^5\text{-}C_5H_5)(CO)_2I]$ (0.70 g, 2.0 mmol) in thf (100 cm^3) was stirred at 328 K for 18 h. The solvent was removed on a rotary evaporator and the residue, after being dissolved in the minimum quantity of CH_2Cl_2, was adsorbed onto silica. The silica was pumped dry and added to the top of a 3 cm × 30 cm chromatography column (Kieselgel 60, 70–230 mesh). Elution with hexane–dichloromethane (3:1) gave $[RuMn(\eta^5\text{-}C_5H_5)(CO)_7]$ **1** (0.59 g, 70%). Recrystallisation from hexane gave **1** as bright yellow crystals (Found: C, 34.8; H, 1.2. $C_{12}H_5MnO_7Ru$ requires C, 34.5; H, 1.2%). Mass spectrum: *m/z* 418 (M^+) and $M^+ - nCO$ (n = 1–7). $\nu_{max}(CO)$ (hexane) at 2082m, 2011w, 2000s, 1988s, 1972s and 1955w cm^{-1}. NMR ($CDCl_3$): ^1H, δ 5.25 (s, 5 H, C_5H_5); ^{13}C (243 K, ^1H composite pulse decoupled), δ 216 (s, br, 7CO) and 86.7 (s, C_5H_5).

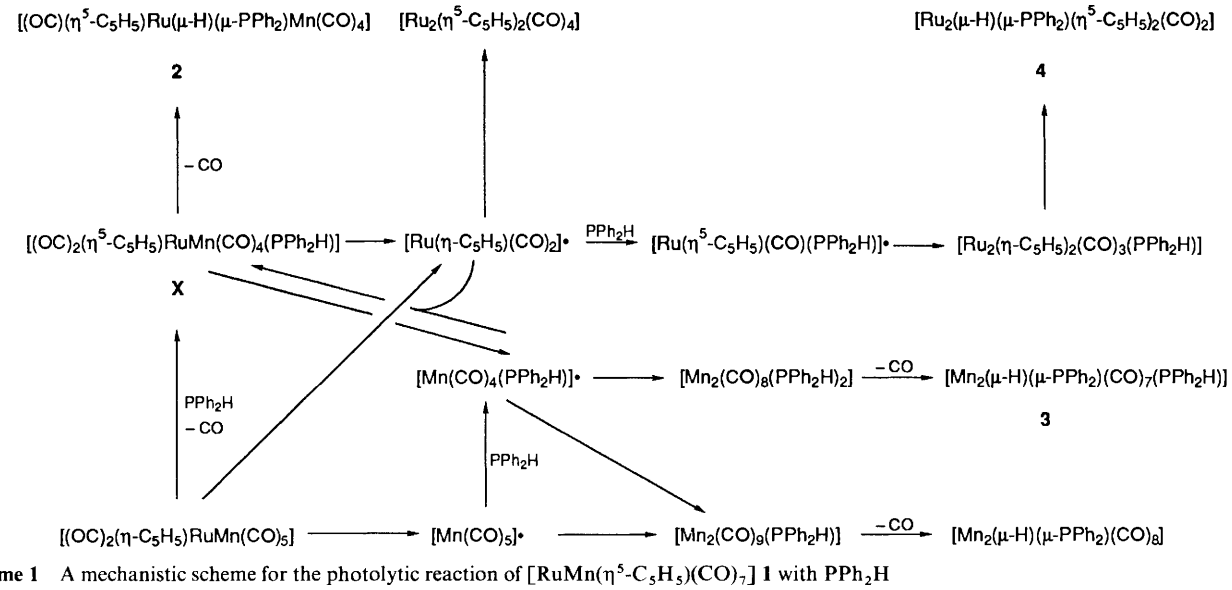

Scheme 1 A mechanistic scheme for the photolytic reaction of $[RuMn(\eta^5\text{-}C_5H_5)(CO)_7]$ **1** with PPh_2H

Reaction of Complex **1** *with* PPh_2H.—(*a*) *Thermolytic reaction.* A solution of complex **1** (0.030 g, 0.072 mmol) and PPh_2H (0.013 cm^3, 0.075 mmol) in toluene (40 cm^3) was heated at 353 K for 4 h. Infrared spectroscopy indicated the presence of **1** and no new products. The solution was heated under reflux for 18 h. Spot TLC and IR spectroscopy showed only the presence of decomposition material together with traces of $[Ru_2(\eta^5\text{-}C_5H_5)_2(CO)_4]$.

(*b*) *Photolytic reaction.* In a typical reaction, a solution of complex **1** (0.46 g, 1.1 mmol) and PPh_2H (0.38 cm^3, 2.2 mmol) in toluene (50 cm^3) was irradiated with UV light for 1 h. The solution changed from yellow to dark orange during this time. The solvent was removed on a rotary evaporator and the residue, after being dissolved in the minimum of dichloromethane, was applied to the base of TLC plates. Elution with hexane–dichloromethane (3:1) gave (decreasing R_f values) $[Mn_2(\mu\text{-}H)(\mu\text{-}PPh_2)(CO)_8]$ (0.025 g), orange crystalline $[RuMn(\mu\text{-}H)(\mu\text{-}PPh_2)(\eta^5\text{-}C_5H_5)(CO)_5]$ **2** (0.040 g, 7%), yellow crystalline $[Mn_2(\mu\text{-}H)(\mu\text{-}PPh_2)(CO)_7(PPh_2H)]$ **3** (0.046 g, 12%), orange crystalline *trans*-$[Ru_2(\mu\text{-}H)(\mu\text{-}PPh_2)(\eta^5\text{-}C_5H_5)_2(CO)_2]$ **4a** (0.012 g, 4%), orange crystalline *cis*-$[Ru_2(\mu\text{-}H)(\mu\text{-}PPh_2)(\eta^5\text{-}C_5H_5)_2(CO)_2]$ **4b** (0.008 g, 3%), orange crystalline $[RuMn_2(\mu\text{-}H)(\mu\text{-}PPh_2)_2(\eta^5\text{-}C_5H_5)(CO)_9]$ **5** (0.135 g, 27%), orange crystalline $[RuMn_2(\mu\text{-}H)(\mu\text{-}PPh_2)_2(\eta^5\text{-}C_5H_5)(CO)_8(PPh_2H)]$ **6** (0.049, 8%) and $[Ru_2(\eta^5\text{-}C_5H_5)_2(CO)_4]$ (0.068 g). A number of other minor bands were observed but not isolated.

Complex **2** (Found: C, 48.9; H, 3.1. $C_{22}H_{16}MnO_5PRu$ requires C, 48.3; H, 2.9%). Mass spectrum: *m/z* 548 (M^+) and $M^+ - n$CO (n = 1–5). ν_{max}(CO) (hexane) at 2069s, 1996s, 1978s and 1952s cm^{-1}. NMR: ^1H (CD_2Cl_2), δ 7.9–7.3 (m, 10 H, Ph), 5.03 (s, 5 H, C_5H_5) and −15.00 [d, 1 H, ^2J(PH) 22, Ru(μ-H)Mn]; ^{13}C (CD_2Cl_2, 215 K, ^1H composite pulse decoupled), δ 219.8 [s, 1 Mn(CO)], 218.9 [s, 1 Mn(CO)], 212.0 [d, ^2J(PC) 16, 1 Mn(CO)], 210.4 [d, ^2J(PC) 13, 1 Mn(CO)], 201.0 [d, ^2J(PC) 12 Hz, Ru(CO)], 143–128 (m, Ph) and 85.2 (s, C_5H_5); (at 298 K) δ 201.0 [s, Ru(CO)], 143–128 (m, Ph) and 85.2 (s, C_5H_5); $^{31}P(CDCl_3$, ^1H-gated decoupled), δ 23.8 (s, μ-PPh_2).

Complex **3** (Found: C, 53.3; H, 3.40. $C_{31}H_{22}Mn_2O_7P_2$ requires C, 54.2; H, 3.2%). Mass spectrum: *m/z* 678 (M^+) and $M^+ - n$CO (n = 1–7). ν_{max}(CO) (hexane) at 2076w, 2026w, 1996s, 1953m and 1930w cm^{-1}. NMR: $^1H(CD_3COCD_3)$, δ 8.0–7.3 (m, 20H, Ph), 7.38 [dd, 1 H, ^1J(PH) 359.5, ^3J(PH) 1.4, PPh_2H] and −16.26[dd, 1 H, ^2J(PH), ^2J(P′H) 29.8 Hz, Mn(μ-H)Mn]; $^{31}P(CDCl_3$, ^1H-gated decoupled), δ 24.4 (s, μ-PPh_2) and −95.9 (s, PPh_2H).

Complex **4a** (Found: C, 49.5; H, 3.6. $C_{24}H_{21}O_2PRu_2$ requires C, 50.1; H, 3.7%). Mass spectrum: *m/z* 576 (M^+) and $M^+ - n$CO (n = 1 or 2) ν_{max}(CO) (CH_2Cl_2) at 1919s cm^{-1}. NMR ($CDCl_3$) ^1H, δ 7.7–7.2 (m, 10 H, Ph), 4.87 (s, 10 H, C_5H_5) and −14.80 [d, 1 H, ^2J(PH) 21 Hz, Ru(μ-H)Ru]; $^{31}P(^1H$-gated decoupled), δ 24.7 (s, μ-PPh_2).

Complex **4b** (Found: C, 49.8; H, 3.9). Mass spectrum: *m/z* 576 (M^+) and $M^+ - n$CO (n = 1 or 2) ν_{max}(CO)(CH_2Cl_2) at 1956s cm^{-1}. Proton NMR ($CDCl_3$): δ7.0–6.9 (m, 10 H, Ph), 5.01 (s, 10 H, C_5H_5) and −14.81[d, 1 H, ^2J(PH) 22 Hz, Ru(μ-H)Ru].

Complex **5** (Found: C, 50.7; H, 2.8; P, 7.2. $C_{38}H_{26}Mn_2O_9P_2Ru$ requires C, 50.7; H, 2.9; P, 6.9%) FAB mass spectrum: *m/z* 900 (M^+) and $M^+ - n$CO (n = 1–9). ν_{max}(CO) (hexane) at 2072m, 2038s, 2016m, 1993s, 1949s, 1927m and 1896w cm^{-1}. NMR: ^1H (CD_2Cl_2), δ 7.9–7.2 (m, 20 H, Ph), 5.17 (s, 5 H, C_5H_5) and −15.68[dd, 1 H, ^2J(PH) 30.7, ^2J(P′H) 23.3 Hz, Mn(μ-H)Mn]; $^{31}P(CDCl_3$, ^1H-gated decoupled), δ 26.4 [s, Mn(μ-PPh_2)Mn] and −97.4 [s, Mn(μ-PPh_2)Ru].

Complex **6** (Found: C, 55.0; H, 3.50. $C_{49}H_{37}Mn_2O_8P_3Ru$

Table 4 Crystal data, data collection, and processing parameters* for complexes **2**, **4a** and **5**

Compound	**2**	**4a**	**5**
Formula	$C_{22}H_{16}MnO_5PRu$	$C_{24}H_{21}O_2PRu_2$	$C_{38}H_{26}Mn_2O_9P_2Ru$
M	547.33	574.52	899.48
Crystal system	Monoclinic	Orthorhombic	Orthorhombic
a/Å	10.851(2)	10.905(6)	9.447(1)
b/Å	14.126(2)	12.264(7)	23.282(1)
c/Å	14.477(2)	16.257(9)	34.248(6)
β/°	102.54(1)	90.0	90.0
U/Å^3	2166.1	2174.2	7532.7
D_c/g cm^{-3}	1.678	1.755	1.586
Z	4	4	8
Space group	$P2_1/n$ [non-standard setting of $P2_1/c$(no. 14)]	*Pnan* [non-standard setting of *Pnna* (no. 52)]	*Pbca* (no. 61)
Colour	Dark red	Orange	Orange
Dimensions/mm	0.129 × 0.228 × 0.228	0.082 × 0.228 × 0.448	0.087 × 0.133 × 0.484
F(000)	1088	1136	3376
μ(Mo-Kα)/cm^{-1}	13.14	14.22	11.18
No. of reflections used to determine cell	56	50	62
Collection mode	ω–θ	ω–θ	ω
Step width (ω)	0.04	0.02	0.04
No. steps per scan	24	30	24
Scan time per step/s	0.75–3.0	0.81–3.0	1.0–4.0
2θ limits/°	5–45	5–50	5–45
Index limits	$-h, +k, \pm l$	$+h, +k, -l$	$-h, +k, -l$
No. of reflections measured	3154	2209	5573
No. of unique reflections	2830	1826	4910
Merging *R*	0.019	0.010	0.010
No. reflections with $F > 4\sigma(F)$	2276	1655	3543
Transmission factors (max., min)	0.879, 0.699	0.894, 0.797	0.897, 0.851
g in $w = 1/[\sigma^2(F_o) + gF_o^2]$	0.000 108	0.001	0.000 184
R	0.040	0.030	0.052
R′	0.039	0.037	0.048
Residual peaks (max., min.) in final difference map/e Å^{-3}	0.994, −0.401	0.678, −0.621	0.698, −0.525
Maximum shift/e.s.d. in final cycle	0.002	0.121	0.020

* All data were collected. Details in common: crystal habit, block; λ(Mo-Kα) 0.710 69 Å; Stoe diffractometer; 2θ range 20–25°; numerical absorption correction.[35]

requires C, 55.6; H, 3.50%) FAB mass spectrum: m/z 1058 (M^+) and $M^+ - n$CO (n = 3–8) ν_{max}(CO) (hexane) at 2069m, 2013m, 1990s, 1944s, 1920m and 1893w cm^{-1}. NMR: ^{1}H-(CD_2Cl_2), δ 7.9–7.0 (m, 30 H, Ph), 6.46 [dd, 1 H, ^1J(PH) 377, ^3J(PH) 11.9, PPh_2H], 4.87 (s, 5 H, C_5H_5) and −15.48 (dd, 1 H, ^2J(PH) 32, ^2J(P'H) 21, Mn(μ-H)Mn]; ^{31}P ($CDCl_3$), δ 25.6 [s, Mn(μ-PPh_2)Mn], −102.1 [d, ^1J(PH) 380 Hz, PPh_2H] and −106.4 [s, Mn(μ-PPh_2)Ru]; ($CDCl_3$, ^{1}H-gated decoupled) δ 25.6 [s, Mn(μ-PPh_2)Mn], −102.1 (s, PPh_2H) and −106.4 [s, Mn(μ-PPh_2)Ru].

Table 5 Atomic coordinates (× 10^4) for complex **2**

Atom	x	y	z
Ru	7 971(1)	8 442(1)	5 389(1)
Mn	8 286(1)	6 419(1)	5 652(1)
P	9 214(1)	7 625(1)	6 597(1)
C(102)	8 209(3)	7 184(2)	8 190(3)
C(103)	7 924	7 386	9 064
C(104)	8 327	8 235	9 523
C(105)	9 015	8 882	9 109
C(106)	9 300	8 681	8 236
C(101)	8 897	7 832	7 776
C(112)	11 687(4)	6 928(2)	7 112(3)
C(113)	13 000	7 007	7 348
C(114)	13 570	7 888	7 318
C(115)	12 827	8 690	7 051
C(116)	11 515	8 611	6 815
C(111)	10 945	7 730	6 845
C(1)	7 151(7)	9 869(5)	5 093(6)
C(2)	7 307(7)	9 694(5)	6 054(6)
C(3)	6 516(8)	8 934(6)	6 161(6)
C(4)	5 889(6)	8 658(5)	5 275(8)
C(5)	6 262(7)	9 235(6)	4 592(5)
C(11)	9 283(6)	8 629(4)	4 789(4)
O(11)	10 070(5)	8 794(4)	4 393(3)
C(21)	9 679(6)	6 399(4)	5 107(4)
O(21)	10 514(5)	6 368(4)	4 757(4)
C(22)	7 480(6)	5 695(4)	4 663(4)
O(22)	7 016(4)	5 201(3)	4 055(3)
C(23)	6 817(6)	6 464(4)	6 108(4)
O(23)	5 921(4)	6 447(3)	6 378(3)
C(24)	8 905(6)	5 484(5)	6 446(4)
O(24)	9 314(5)	4 901(3)	6 975(3)

Crystal Structure Determination and Refinements.—Suitable crystals of the compounds were mounted on glass fibres with epoxy resin. Details of crystal data, data collection and refinement parameters are given in Table 4.

The Ru atoms in each of the three structures were located from Patterson syntheses, and the Mn atoms in structures **2** and **5** and the remaining non-hydrogen atoms were located from subsequent Fourier difference syntheses. The bridging hydride ligands were also located directly in the difference maps and were refined freely during the refinement processes. The remaining hydrogen atoms were placed in idealised positions (C–H 1.08 Å) and allowed to ride on the relevant carbon atoms; each type of hydrogen was assigned a common isotropic thermal parameter. For structures **2** and **5** the phenyl rings were refined as rigid groups with C–C set at 1.395 Å and C–C–C at 120°. The structures were refined to convergence by full-matrix least squares (for **4a**) and blocked full-matrix least squares (for **2** and **5**) with all non-hydrogen atoms assigned anisotropic thermal parameters for **4a**, and all non-hydrogen atoms except the phenyl carbons for **2** and **5**. Weighting schemes were applied, and analyses of the variations of the sum of $w\Delta^2$ [$\Delta = F_o - |F_c|$)] according to $|F_o|$ and sin θ indicated that the schemes were appropriate. The final residuals were calculated on the

Table 6 Atomic coordinates (× 10^4) for complex **4a**

Atom	x	y	z
Ru(1)	1193(1)	2109(1)	−178(1)
P	2500	3554(1)	0
C(1)	777(4)	1940(3)	921(3)
O(1)	444(4)	1769(3)	1577(2)
C(11)	2431(3)	4510(3)	866(2)
C(12)	1578(4)	4400(3)	1492(3)
C(13)	1589(4)	5101(3)	2172(3)
C(14)	2424(4)	5914(3)	2230(3)
C(15)	3266(4)	6059(3)	1596(3)
C(16)	3259(4)	5360(3)	924(3)
C(2)	390(5)	2654(4)	−1389(3)
C(3)	1110(6)	1782(7)	−1547(3)
C(4)	696(6)	888(5)	−1163(3)
C(5)	−342(5)	1139(5)	−723(3)
C(6)	−580(5)	2289(6)	−833(4)

Table 7 Atomic coordinates (× 10^4) for complex (**5**)

Atom	x	y	z
Ru	−1262(1)	6234(1)	1090(1)
Mn(1)	−54(1)	4570(1)	1205(1)
Mn(2)	2445(1)	3916(1)	1477(1)
P(1)	608(2)	5544(1)	1154(1)
C(101)	1672(5)	5826(2)	1567(2)
C(102)	1705	5538	1924
C(103)	2546	5746	2228
C(104)	3356	6241	2174
C(105)	3323	6528	1817
C(106)	2482	6321	1513
C(111)	1943(4)	5615(2)	759(1)
C(112)	1590	5798	384
C(113)	2616	5803	91
C(114)	3994	5626	173
C(115)	4346	5443	549
C(116)	3321	5437	842
P(2)	199(2)	3628(1)	1311(1)
C(201)	−864(4)	3285(2)	1696(1)
C(202)	−225	2888	1945
C(203)	−1013	2630	2241
C(204)	−2440	2768	2288
C(205)	−3079	3164	2038
C(206)	−2291	3423	1742
C(211)	−68(4)	3101(2)	917(1)
C(212)	944	2679	840
C(213)	703	2273	548
C(214)	−550	2288	333
C(215)	−1563	2709	410
C(216)	−1322	3116	702
C(1)	−2582(13)	6901(4)	1395(3)
C(2)	−1536(11)	6695(4)	1655(3)
C(3)	−1809(11)	6119(4)	1725(2)
C(4)	−2974(11)	5953(4)	1506(3)
C(5)	−3446(11)	6443(6)	1298(3)
C(11)	−88(10)	6768(4)	843(3)
O(11)	571(7)	7117(3)	702(2)
C(12)	−1833(9)	5902(4)	617(3)
O(12)	−2283(7)	5709(3)	334(2)
C(21)	431(8)	4467(3)	692(2)
O(21)	628(7)	4404(2)	363(2)
C(22)	−1846(9)	4605(3)	1037(2)
O(22)	−3000(6)	4599(3)	933(2)
C(23)	−809(8)	4666(3)	1691(2)
O(23)	−1397(7)	4734(2)	1979(2)
C(31)	4021(9)	4351(3)	1593(3)
O(31)	4981(7)	4610(3)	1681(2)
C(32)	3092(9)	3838(4)	970(3)
O(32)	3516(7)	3791(3)	662(2)
C(33)	3193(9)	3237(4)	1596(3)
O(33)	3659(7)	2789(2)	1667(2)
C(34)	1823(9)	4022(3)	1986(3)
O(34)	1486(8)	4103(3)	2296(2)

basis $R = [\Sigma||F_o| - |F_c||/\Sigma F_o]$, $R' = \Sigma w^{\frac{1}{2}}||F_o| - |F_c||/\Sigma w^{\frac{1}{2}}F_o]$, and $w = 1/[\sigma^2(F_o) + gF_o^2]$ where $\sigma(F_o)$ is calculated from counting statistics. The final positional coordinates for all the non-hydrogen atoms in **2**, **4a** and **5** are listed in Tables 5–7 respectively. All atoms were assigned complex neutral-atom scattering factors which were taken from ref. 36. Calculations were performed on the University of Cambridge IBM 3084Q mainframe computer using SHELX 76.[35] Structural diagrams were drawn using the SHELXTL PLUS package.[37]

Additional material available from the Cambridge Crystallographic Data Centre comprises H-atom coordinates, thermal parameters, and remaining bond lengths and angles.

Acknowledgements

We thank Dr. A. G. Kent for valuable discussion, and the SERC and BP Chemicals Limited (Hull division) for financial support.

References

1 A. J. Carty, *Adv. Chem. Ser.*, 1982, **196**, 163; *Pure Appl. Chem.*, 1982, **54**, 113.
2 D. A. Roberts and G. L. Geoffroy, in *Comprehensive Organometallic Chemistry*, eds. G. Wilkinson, F. G. A. Stone and E. W. Abel, Pergamon, London, 1982, ch. 40.
3 P. M. Treichel, W. K. Dean and W. M. Douglas, *Inorg. Chem.*, 1972, **11**, 1609.
4 B. E. Hanson, P. E. Fanwick and J. S. Mancini, *Inorg. Chem.*, 1982, **21**, 3811.
5 J. A. Iggo, M. J. Mays, P. R. Raithby and K. Henrick, *J. Chem. Soc., Dalton Trans.*, 1983, 205.
6 R. B. King, W-K. Fu and E. M. Holt, *J. Chem. Soc., Chem. Commun.*, 1984, 1439.
7 H.-J. Haupt, P. Balsaa and U. Flörke, *Z. Anorg. Allg. Chem.*, 1987, **548**, 151.
8 K. Henrick, M. McPartlin, A. D. Horton and M. J. Mays, *J. Chem. Soc., Dalton Trans.*, 1988, 1083.
9 A. D. Horton, M. J. Mays and P. R. Raithby, *J. Chem. Soc., Dalton Trans.*, 1987, 1557.
10 T. Adatia, K. Henrick, A. D. Horton, M. J. Mays and M. McPartlin, *J. Chem. Soc., Chem. Commun.*, 1986, 1206.
11 A. D. Horton, A. C. Kemball and M. J. Mays, *J. Chem. Soc., Dalton Trans.*, 1988, 2953.
12 A. D. Horton, M. J. Mays, and P. R. Raithby, *J. Chem. Soc., Chem. Commun.*, 1985, 247.
13 R. B. King, P. M. Treichel and F. G. A. Stone, *Chem. Ind. (London)*, 1961, 747.
14 S. A. R. Knox, R. J. McKinney and F. G. A. Stone, *J. Chem. Soc., Dalton Trans.*, 1980, 235.
15 K. R. Pope and M. S. Wrighton, *J. Am. Chem. Soc.*, 1987, **109**, 4545.
16 M. L. H. Green and J. T. Moelwyn-Hughes, *Z. Naturforsch., Teil B*, 1962, **17**, 783.
17 E. O. Fisher and A. Vogler, *Z. Naturforsch., Teil B*, 1962, **17**, 421.
18 R. P. Rosen, J. B. Hoke, R. R. Whittle, G. L. Geoffroy, J. P. Hutchinson and J. A. Zubieta, *Organometallics*, 1984, **3**, 846.
19 R. J. Doedens, W. T. Robinson and J. A. Ibers, *J. Am. Chem. Soc.*, 1967, **89**, 4323.
20 J. Schneider, L. Zsolnai and G. Huttner, *Chem. Ber.*, 1982, **115**, 989.
21 J. A. Iggo, M. J. Mays, P. R. Raithby and K. Henrick, *J. Chem. Soc., Dalton Trans.*, 1984, 633.
22 (*a*) S. W. Carr and B. L. Shaw, *Polyhedron*, 1987, **6**, 11; (*b*) T. A. Pakkanen, J. Pursiainen, T. Venäläinen and T. T. Pakkanen, *J. Organomet. Chem.*, 1989, **372**, 129.
23 O. S. Mills and J. P. Nice, *J. Organomet. Chem.*, 1967, **9**, 339.
24 A. F. Dyke, S. A. R. Knox, M. J. Morris and P. J. Naish, *J. Chem. Soc., Dalton Trans.*, 1983, 1417.
25 R. G. Hayter, *J. Am. Chem. Soc.*, 1963, **85**, 3120.
26 M. Creswick, I. Bernal, B. Reiter and W. A. Herrmann, *Inorg. Chem.*, 1982, **21**, 645.
27 D. J. Brauer, G. Hasselkuss, S. Morton, S. Hietkamp, H. Sommer, O. Stelzer and W. S. Sheldrick, *Z. Naturforsch., Teil B*, 1985, **40**, 1161.
28 G. Johannsen and P. Stelzer, *Chem. Ber.*, 1977, **110**, 3438.
29 J. L. Petersen and R. P. Stewart, jun., *Inorg. Chem.*, 1980, **19**, 186.
30 P. E. Garrou, *Chem. Rev.*, 1981, **81**, 229.
31 A. J. Carty, S. A. MacLaughlin and D. Nucciarone, *Methods in Stereochemical Analysis*, eds. J. G. Verkade and L. D. Quin, VCH, Deerfield Beach, FL, 1987, vol. 8, p. 559.
32 H. B. Abrahamson, M. C. Palazzotto, C. L. Reichel and M. S. Wrighton, *J. Am. Chem. Soc.*, 1979, **101**, 4123.
33 R. B. King and F. G. A. Stone, *Inorg. Synth.*, 1963, **7**, 196.
34 R. J. Haines and A. L. du Preez, *J. Chem. Soc., Dalton Trans.*, 1972, 944.
35 G. M. Sheldrick, SHELX 76, Crystal Structure Determination Package, University of Cambridge, 1976.
36 *International Tables for X-Ray Crystallography*, Kynoch Press, Birmingham, 1974, vol. 4.
37 Release 4.0 of SHELXTL PLUS, Siemens Analytical X-Ray Instruments, Inc., Siemens Part No. 269–004200, 1990.

Received 21*st January* 1991; *Paper* 1/00279A